CHANG, C. & BADER, R. F. W. (1992). *J. Phys. Chem.* **96**, 1654–1662.
CIOSLOWSKI, J. & MCKEE, M. L. (1992). *J. Phys. Chem.* **96**, 9264–9268.
CIOSLOWSKI, J. & MIXON, S. T. (1992). *Can. J. Chem.* **70**, 443–449.
CIOSLOWSKI, J., MIXON, S. T. & EDWARDS, W. D. (1991). *J. Am. Chem. Soc.* **113**, 1083–1085.
COLLIN, R. L. (1952). *Acta Cryst.* **5**, 431–432; erratum (1956), **9**, 537.
COX, S. R., HSU, L. Y. & WILLIAMS, D. E. (1981). *Acta Cryst.* A**37**, 293–301.
CREMER, D., KRAKA, E., SLEE, T. S., BADER, R. F. W., LAU, C. D. H., NGUYEN-DANG, T. T. & MACDOUGALL, P. J. (1983). *J. Am. Chem. Soc.* **105**, 5069–5075.
DESTRO, R., BIANCHI, R., GATTI, C. & MERATI, F. (1991). *Chem. Phys. Lett.* **186**, 47–52.
DONOHUE, J. & GOODMAN, S. H. (1965). *Acta Cryst.* **18**, 568–569.
DOWNS, J. W. & SWOPE, R. J. (1992). *J. Phys. Chem.* **96**, 4834–4840.
DUNITZ, J. D. & SEILER, P. (1983). *J. Am. Chem. Soc.* **105**, 7056–7058.
EBERHART, M. E., CLOUGHERTY, D. P. & MACLAREN, J. M. (1993). *J. Mater. Res.* **8**, 438–448.
EBERHART, M. E., DONOVAN, M. M., MACLAREN, J. M. & CLOUGHERTY, D. P. (1991). *Prog. Surf. Sci.* **36**, 1–34.
EBERHART, M. E., DONOVAN, M. M. & OUTLAW, R. A. (1992). *Phys. Rev. B*, **46**, 12744–12747.
FRISCH, M. J., TRUCKS, G. W., HEAD-GORDON, M., GILL, P. M. W., WONG, M. W., FORESMAN, J. B., JOHNSON, B. G., SCHLEGEL, H. B., ROBB, M. A., REPLOGLE, E. S., GOMPERTS, R., ANDRES, J. L., RAGHAVACHARI, K., BINKLEY, J. S., GONZALEZ, C., MARTIN, R. L., FOX, D. J., DEFREES, D. J., BAKER, J., STEWART, J. J. P. & POPLE, J. A. (1992). Gaussian, Inc., Pittsburgh, PA, USA.
HAHN, T. (1983). *International Tables for Crystallography*, Vol. A. Boston: Kluwer Academic Publishers.
HANSEN, N. K. & COPPENS, P. (1978). *Acta Cryst.* A**34**, 909–921.
HSU, L. Y. & WILLIAMS, D. E. (1979). *Inorg. Chem.* **18**, 79–82.
KAPPHAHN, M., TSIRELSON, V. G. & OZEROV, R. P. (1988). *Port. Phys.* **19**, 213–216.
LOW, A. A., KUNZE, K. L., MACDOUGALL, P. J. & HALL, M. B. (1991). *Inorg. Chem.* **30**, 1079–1086.
MACDOUGALL, P. J. & HALL, M. B. (1990). *Trans. Am. Crystallogr. Assoc.* **26**, 105–123.
MEI, C., EDGECOMBE, K. E., SMITH, V. H. & HEILINGBRUNNER, A. (1993). *Int. J. Quantum Chem.* **48**, 287–293.
MILLS, R. L. & SCHUCH, A. F. (1969). *Phys. Rev. Lett.* **23**, 1154–1156.
NYBURG, S. C. (1979). *Acta Cryst.* A**35**, 641–645.
NYBURG, S. C. & WONG-NG, W. (1979). *Inorg. Chem.* **18**, 2790–2791.
PISANI, C., DOVESI, R. & ORLANDO, R. (1992). *Int. J. Quantum Chem.* **42**, 5–33.
PISANI, C., DOVESI, R. & ROETTI, C. (1988). *Hartree–Fock Ab Initio Treatment of Crystalline Systems, Lecture Notes in Chemistry*, Vol. 48. Heidelberg: Springer-Verlag.
POPELIER, P. L. A. & BADER, R. F. W. (1992). *Chem. Phys. Lett.* **189**, 542–548.
POPELIER, P. L. A. & BADER, R. F. W. (1994). *J. Phys. Chem.* **98**, 4473–4481.
RAICH, J. C. & MILLS, R. L. (1971). *J. Chem. Phys.* **55**, 1811–1817.
SCHIFERL, D., CROMER, D. T., SCHWALBE, L. A. & MILLS, R. L. (1983). *Acta Cryst.* B**39**, 153–157.
SCHUCH, A. F. & MILLS, R. F. (1970). *J. Chem. Phys.* **52**, 6000–6008.
STEVENS, E. D. (1979). *Mol. Phys.* **37**, 27–45.
STEWART, R. F. (1991). *The Application of Charge Density Research to Chemistry and Drug Design*, edited by G. A. JEFFREY & J. F. PINIELLA, pp. 63–102. NATO ASI Series B, No. 250.
WIBERG, K. B., BADER, R. F. W. & LAU, C. D. H. (1987). *J. Am. Chem. Soc.* **109**, 985–1000.
WILLIAMS, D. E. & COX, S. R. (1984). *Acta Cryst.* B**40**, 404–417.
WILLIAMS, D. E. & HSU, L.-Y. (1985). *Acta Cryst.* A**41**, 296–301.
WILLIAMS, D. E. & WELLER, R. R. (1983). *J. Am. Chem. Soc.* **105**, 4143–4148.
YAMASAKI, K. (1962). *J. Chem. Soc. Jpn*, **17**, 1262–1267.
ZOU, P. F. & BADER, R. F. W. (1994). *Acta Cryst.* A**50**, 714–725.

Acta Cryst. (1995). A**51**, 153–158

Simulation of Short-Range Order in F.C.C. Alloys

BY S. H. RAHMAN AND M. RODEWALD*

Institut für Mineralogie, Universität Hannover, Welfengarten 1, 30167 *Hannover, Germany*

(*Received* 22 *March* 1994; *accepted* 1 *August* 1994)

Abstract

The videographic simulation algorithm has been further developed to enable any distribution or vector correlation among atoms or structure variants beyond the first shell. The simulation method is applied to Ni_4Mo, Au_4Mn and Cu_3Au in order to describe their real structures above T_c. One of the main advantages of the method is the rapid calculation of the diffraction pattern from the simulated videographic structure image (parallel processing). Moreover, the 3D simulation field can be analysed to determine the local atomic arrangement or to calculate short-range-order parameters. The method can generally be applied to simulate defect or vacancy distributions with a specific degree of correlation.

Introduction

In order to characterize the local atomic arrangement of an alloy above the critical temperature (T_c), the Warren–Cowley short-range-order parameters a_{lmn} are used (Cowley, 1950).

To assist in the interpretation of the atomic configuration for the short-range-ordered state of alloys, Gehlen & Cohen (1965) conducted computer simulations based on experimentally measured short-range-order parameters (a_{lmn}). These Monte Carlo simulations were

* Present address: Fachbereich Materialwissenschaften, Fachgebiet Strukturforschung, Technische Hochschule Darmstadt, Petersenstrasse 20, 64287 Darmstadt, Germany.

performed using the first three a_{lmn}. In the simulations, the positions of the atoms (4000–16000) were first selected randomly and then interchanged until the best fit was obtained between the experimental and calculated values of a_{lmn}. A similar procedure involving considerably shorter computing times was developed by Williams (1970). Monte Carlo simulations based on particle interactions were also carried out by Golosov & Dudka (1973), Polgreen (1985), Gompper & Kroll (1988) and Zhu & Zabel (1990).

More recently, a computer simulation method (the videographic method) using combination probabilities (W_{ij}) to distribute a set of atoms or structure variants in order to describe the real structure configuration was developed by Rahman (1993*a*). The method was first applied to describe the real structure of Cu_3Au at different temperatures (Rahman, 1993*b*, 1994*a*). An essential advantage of the videographic method is the possibility of calculating the Fourier transform (diffraction pattern) from the simulated videographic real-structure image for comparison with experimental results. Moreover, in the special case of short-range ordering, the a_{lmn} values can be calculated from the simulated model and compared with experimental data. The determination of the combination probabilities W_{ij} used for the distribution of atoms or structure variants follow, in this case, a trial-and-error procedure and can only be determined empirically. However, the combination probabilities are influenced by conditional probabilities. The conditional probabilities are produced through prohibited combinations between structure variants or atoms. Hence, a determination of the correct set of W_{ij} is somewhat difficult because of the possible differences between the input probability values and those calculated from the simulation field which includes implicitly the conditional probabilities.

In the present paper, the videographic simulation algorithm is further developed to facilitate an easier access to any distance correlation (vector correlation) as well as combination probabilities and to reduce the influence of conditional probabilities.

The simulation procedure is applied to Ni_4Mo, Au_4Mn and Cu_3Au to describe the local atomic configuration above the critical temperature (T_c).

Simulation procedure

In order to simulate a real structure, a certain set of n structure variants $\varphi_j(x, y, z)$ containing one or more atoms must be derived from the average structure. These structure variants are distributed using a random variable J taking the values j ($j = 1, \ldots, n$) with certain probabilities determined by the distribution function of J (Rahman, 1993*a*). The distribution function is defined in terms of the combination probabilities W_{ji} for all simulation directions as shown in Table 1 for the [100] direction (j and i are the suffices of the tables or stochastic matrices).

Table 1. *Scheme for the combination probabilities in the* [100] *direction*

	$\varphi_1(x, y, z)$	$\varphi_2(x, y, z)$	...	$\varphi_n(x, y, z)$
$\varphi_1(x, y, z)$	W_{11}	W_{12}		W_{1n}
$\varphi_2(x, y, z)$	W_{21}	W_{22}		W_{2n}
⋮	⋮	⋮		⋮
$\varphi_n(x, y, z)$	W_{n1}	W_{n2}		W_{nn}

The simulation procedure commences at the centre of a three-dimensional simulation field. The first step is the random selection of a single structure variant. This starting variant S has six neighbouring positions within the simulation field to allow a globular growth of the simulation field (Fig. 1). During the simulation, almost every occupation of a location gives rise to new possible locations until the simulation field is completely filled with structure variants.

The evaluation of the combination tables of the neighbouring positions of a selected location gives the probabilities of the structure variants at this location. The selection of a certain structure variant takes place under consideration of the probability of combination. Each structure variant has six possible direct neighbours during the simulation, and hence six combination tables ($CT_{[100]}$, $CT_{[010]}$, $CT_{[001]}$, $CT_{[\bar{1}00]}$, $CT_{[0\bar{1}0]}$, $CT_{[00\bar{1}]}$) are needed in order to fully describe a certain distribution of the $\varphi_j(x, y, z)$. Fig. 1 shows schematically the simulation procedure, which is described in more detail by Rodewald (1993). In order to explain the relationship between the combination tables (CT) in the main directions ($CT_{[100]}$, $CT_{[010]}$, $CT_{[001]}$) and in the opposite directions ($CT_{[\bar{1}00]}$, $CT_{[0\bar{1}0]}$, $CT_{[00\bar{1}]}$), it is convenient to write the combination tables in matrix form:

$$M = \begin{pmatrix} w_{11} & w_{12} & w_{13} & \cdots & w_{1n} \\ w_{21} & w_{22} & w_{23} & \cdots & w_{2n} \\ w_{31} & w_{32} & w_{33} & \cdots & w_{3n} \\ \vdots & \cdots & \cdots & \ddots & \vdots \\ w_{n1} & w_{n2} & w_{n3} & \cdots & w_{nn} \end{pmatrix}.$$

The matrix of the combination table for the opposite direction is the transposed matrix (M^T) of the combination possibilities for the corresponding main direction.

In some cases, especially when short-range ordering is present, it is difficult to influence a certain preference between two structure variants or atoms beyond the first or second shell using the combination tables. This problem occurs particularly in directions with mixed indices (*e.g.* [211], [321]). In order to avoid these difficulties, the combination probabilities given in Table 1 can be manipulated by introducing a set of correlation vectors that controls the probability of any desired combination behind the first shell during the simulation procedure. With the aid of a correlation vector v_{lmn}, a

structure variant A at the position (u, v, w) can directly influence the probability of a structure variant B at the position $(u + l, v + m, w + n)$ within the simulation field (Fig. 1). Therefore, the probability W that a certain structure variant φ of type j is present at the position (u, v, w) is the product of the sum of the probabilities of the combination tables at this position and the influence factors K_{lmn} of all valid correlation vectors V_{lmn} at this position (Rodewald, 1993):

$$W = K_v({}^{[100]}W_{u-1vw} + {}^{[\bar{1}00]}W_{u+1vw} + {}^{[010]}W_{uv-1w} + {}^{[0\bar{1}0]}W_{uv+1w} + {}^{[001]}W_{uvw-1} + {}^{[00\bar{1}]}W_{uvw+1}), \quad (1)$$

where K_v is the product of the influence factors K_{lmn} of all interacting correlation vectors v_{lmn} at the position (u, v, w) and ${}^{[\bar{1}00]}W_{u-1vw}$ is the probability that a structure variant φ of type j occurs, as derived from the corresponding combination table ($CT_{[\bar{1}00]}$) evaluated at the position $(u - 1, v, w)$.

In order to illustrate the effect of reducing the influence of the conditional probabilities, a two-dimensional simulation of disordered Cu_3Au was performed as an example. The corresponding four structure variants $\varphi_j(x, y)$ used for the simulation are presented in a previous paper (Rahman, 1993*b*). The input values of the combination probabilities W_{ji} for the distribution of the four structure variants are given in Table 2 column (*a*) for the [010] direction. The probabilities calculated from the two-dimensional simulation field together with those calculated with the inclusion of the influence factor K_{lmn} in the simulation (1) are given in Table 2, columns (*b*) and (*c*), respectively.

Although the input values W_{13}, W_{24}, W_{31} and W_{42} are set to 1% [Table 2, column (*a*)], the resulting values in the simulation are 14% [Table 2, column (*b*)]. This indicates a considerable preference in the simulation for such combinations. By comparison of the input and output probability values [columns (*a*) and (*c*)], it is observed that the output data calculated by the new simulation algorithm are in much closer agreement with the input data and hence represent more realistic values.

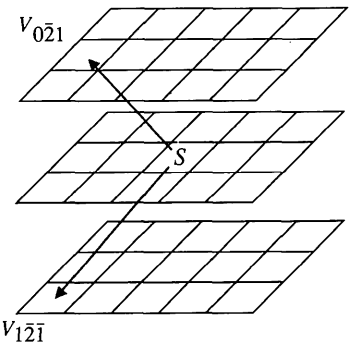

Fig. 1. Schematic illustration of the simulation procedure (S: starting variant, V_{lmn} correlation vector).

Table 2. *Combination probabilities* (%)

(*a*) Input data, (*b*) probabilities calculated in the simulation with the input data (without correction) and (*c*) values calculated in the simulation with the new procedure.

	(*a*)				(*b*)				(*c*)			
	1	2	3	4	1	2	3	4	1	2	3	4
1	0	74	1	25	0	62	14	24	0	72	3	25
2	74	0	25	1	62	0	24	14	72	0	25	3
3	1	25	0	74	14	24	0	62	3	25	0	72
4	25	1	74	0	24	14	62	0	25	3	72	0

In order to simulate short-range ordering in an AB alloy, the experimental short-range-order parameters a_{lmn} (4) can be used to derive the influence factors K_{lmn} for the correlation vectors connecting two atoms of type A (m_A and m_B are the atomic fractions of A and B atoms in the alloy):

$$K_{lmn} = [1 - (1 - \alpha_{lmn})m_B]/m_A. \quad (2)$$

The real 'structure' image $S(U, V, W)$ resulting from a three-dimensional simulation using combination probabilities W_{ji} [Table 1 and equation (1)] and correlation vectors can be expressed as (Rahman, 1993*a*)

$$S(U, V, W) = \sum_u^U \sum_v^V \sum_w^W \varphi_{uvw}(J_{uvw}), \quad (3)$$

where (u, v, w) are integers, $\varphi_{uvw}(J_{uvw})$ is the structure variant of type J at the uvw position and J_{uvw} is the random variable for the uvw position. Different distributions of φ_j can be obtained by varying the values of W (1). Based on the principles of the videographhic simulation method (Rahman, 1993*a*), the structure variants $\varphi_j(x, y, z)$ were replaced by picture elements with different grey levels. The resulting simulation of (3) can be immediately displayed and stored as a videograpic image. To check the result of a simulation, the Fourier transform of the real structure image $S(U, V, W)$ is compared with the experimental diffraction pattern. Moreover, it is possible to evaluate the three-dimensional short-range-order parameters from the simulated three-dimensional model. In contrast to Gehlen & Cohen (1965) and Williams (1970), the simulation field is not obtained by fitting the short-range-order parameters to those obtained from the experiment. In the present procedure, the main control of a simulation is based on a comparison between the diffuse scattering (shape, position and intensity) calculated from the videographic structure image and the experimental diffraction patterns (intensity contour map). Significant errors in the experimental values of a_{lmn} result in changes of the diffuse intensity distribution of the simulated diffraction pattern compared with the experimental diffraction pattern and are therefore conspicuous. Moreover, the

capacity of the applied computer hardware and software enables simulations to be carried out involving up to several million atoms.

Examples

To demonstrate the validity of the above-described simulation procedure, the method was applied to simulate short-range ordering for Ni_4Mo, Au_4Mn and Cu_3Au above T_c. These binary f.c.c. alloys were chosen because their short-range-order parameters have been accurately determined by several authors for the short-range-ordered state [Ni_4Mo: Chakravarti, Starke, Sparks & Williams (1974); Au_4Mn: Fuernrohr, Epperson & Gerold (1980), Suzuki, Harada, Nakashima & Adachi (1982); Cu_3Au: Cowley (1950), Moss (1964), Chen, Comostock & Cohen (1979)].

The short-range-order parameter a_{lmn} can be defined in terms of the probability P_{lmn} that an atom with coordinates lmn with respect to an A atom is also an A atom (Cowley, 1950):

$$a_{lmn} = 1 - (1 - P_{lmn})/m_B. \quad (4)$$

The first set of influence factors K_{lmn} for the correlation vectors used in the simulation were determined using the first six a_{lmn} (2). The calculated values of P_{lmn} and K_{lmn} are given in Table 3.

The structure variants, which contain in this case one atom, are modelled as picture elements for the videographic simulation as shown in Fig. 2(*a*) (Rahman, 1993*a*). The atom-free sequence is used to enable the videographic representation of the sites of the f.c.c. lattice as schematically demonstrated in Fig. 2(*b*). The dimension of the atomic sequences is equal to the unit length of the short-range-order vector r_{lmn}.

The three-dimensional simulation containing 8×10^5 atoms was undertaken using combination probability tables that generate a real structure image of a statistical distribution of two different atoms on the sites of a f.c.c. lattice. The combination probabilities shown in Table 4 are therefore identical for all six

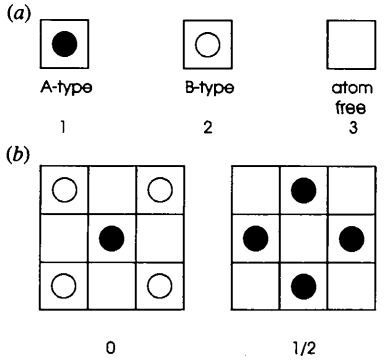

Fig. 2. (*a*) Structure elements ('atoms') for the videographic simulation, and (*b*) structure elements occupying the sites of a f.c.c. lattice.

Table 3. *Calculated values of the probabilities P_{lmn} and the resulting influence factors K_{lmn}*

a_{lmn} from Chakravarti *et al.* (1974), for Ni_4Mo quenched from above T_c; Fuernrohr *et al.* (1980) for Au_4Mn quenched from 873 K; and Chen *et al.* (1979) for Cu_3Au at 669 K.

lmn	P_{Mo-Mo}	K_{Mo-Mo}	P_{Mn-Mn}	K_{Mn-Mn}	P_{Au-Au}	K_{Au-Au}
110	0.0368	0.184	0.0392	0.196	0.118	0.472
200	0.1920	0.960	0.3672	1.826	0.411	1.642
211	0.2912	1.456	0.2416	1.224	0.254	1.015
220	0.1424	0.712	0.1960	0.944	0.297	1.186
310	0.1488	0.744	0.1368	0.672	0.191	0.763
222	0.1016	0.508	0.1224	0.560	0.267	1.066

Table 4. *Scheme for the three-dimensional combination probabilities for the structure variants shown in Fig. 2(a)*

	$\varphi_1(x, y, z)$	$\varphi_2(x, y, z)$	$\varphi_3(x, y, z)$
$\varphi_1(x, y, z)$	0%	0%	100%
$\varphi_2(x, y, z)$	0%	0%	100%
$\varphi_3(x, y, z)$	W_{31}	W_{32}	0%

directions. The values of W_{31} and W_{32} are used to adjust the chemical composition of the simulated binary alloy. The preference of certain combinations between two atoms is taken into account during the simulation by applying the influence factors K given in Table 3.

The Fourier transforms [($hk0$) plane] of the three-dimensional simulations for Ni_4Mo, Au_4Mn and Cu_3Au are shown in Fig. 3. A comparison between the calculated diffraction pattern and the intensity contour map for the short-range-order state measured by several authors [Ni_4Mo: Chakravarti, Starke, Sparks & Williams (1974); Au_4Mn: Fuernrohr, Epperson & Gerold (1980); Cu_3Au: Cowley (1950)] shows quite a good agreement in relation to the characteristic distributions of the diffuse scattering.

In order to characterize the local atomic arrangement of the three alloys, a portion of the first two atomic layers of the videographic image simulations is shown in Fig. 4. The atoms are represented as picture elements (pixels) with different grey levels to model their scattering behaviour. The real structure above T_c can be described as follows: in the case of Ni_4Mo, the structure is not comprised of a distribution of microdomains of the ordered structure $D1_a$ ($I4/m$) as proposed by some authors (*e.g.* Saburi, Kanai & Nenno, 1974). Instead, Ni_4Mo contains small domains of the $D0_{22}$-type ($I4/mmm$) and only fragments of $D1_a$-type domains (Fig. 4). The distribution of the two domain types leads to the characteristic shape of the diffuse intensities. These results are in accordance with a suggestion proposed by Van Tendeloo & Amelinckx (1985).

The diffuse intensity distributions in the reciprocal space of Ni_4Mo and Au_4Mn are similar. In the case of Au_4Mn, the diffuse maxima are slightly elongated towards the main directions (Fig. 3). The Au_4Mn structure contains microdomains of type LI_2 ($Pm3m$) in

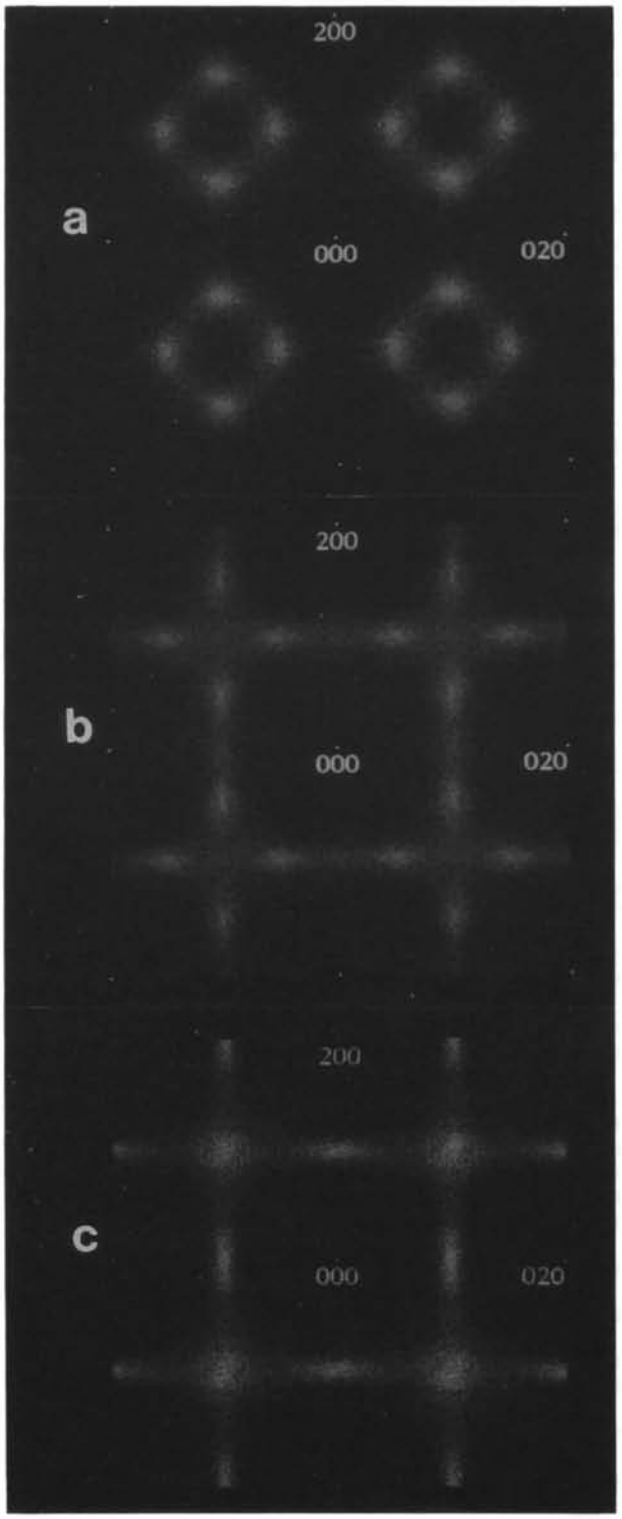

Fig. 3. Fourier transforms [($hk0$) planes] of the three-dimensional simulations (a) Ni_4Mo, (b) Au_4Mn and (c) Cu_3Au.

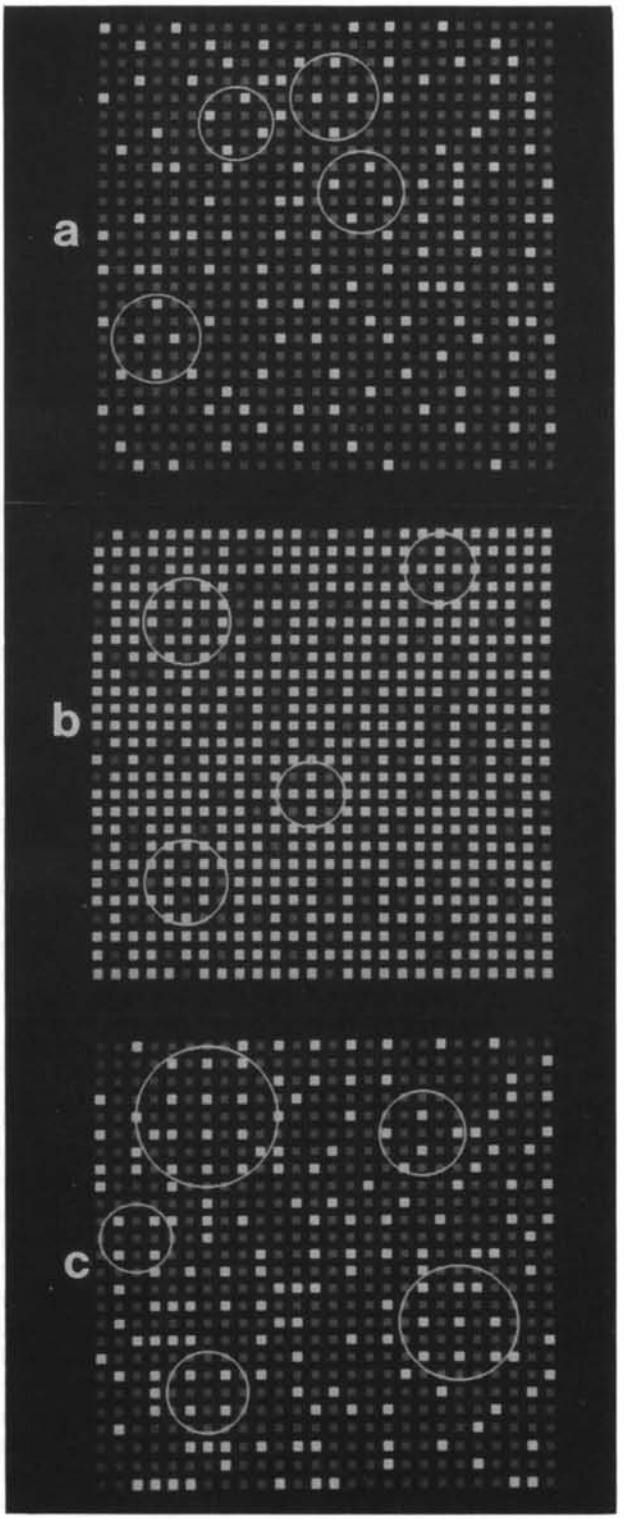

Fig. 4. Sections of the first two atomic layers of the videographic simulations. Several features of the local atomic configuration are circled in the figures. (a) Ni_4Mo, (b) Au_4Mn and (c) Cu_3Au. The grey levels of the pixels are proportional to the atomic number.

Table 5. *Experimental (exp.) and calculated (sim.) a_{lmn} values; the experimental data were taken from the same authors as cited in Table 2*

	Ni_4Mo		Au_4Mn		Cu_3Au	
lmn	a_{lmn} (exp.)	a_{lmn} (sim.)	a_{lmn} (exp.)	a_{lmn} (sim.)	a_{lmn} (exp.)	a_{lmn} (sim.)
110	−0.204	−0.157	−0.201	−0.161	−0.176	−0.162
200	−0.010	0.021	0.207	0.217	0.214	0.224
211	0.114	0.108	0.056	0.042	0.005	0.017
220	−0.072	−0.079	−0.014	−0.001	0.062	0.093
310	−0.064	−0.058	−0.082	−0.104	−0.079	−0.085
222	−0.123	−0.160	−0.110	−0.131	0.022	0.021
321	0.034	0.022	0.035	0.020	−0.010	−0.013
400	0.110	0.111	0.116	0.133	0.073	0.091
330	0.005	−0.069	−0.043	−0.054	−0.030	−0.033
411	−0.046	−0.039	0.000	−0.006	0.026	0.028
420	0.035	0.030	0.012	0.026	0.034	0.042
332	0.013	0.030	0.012	0.021	−0.010	−0.003

addition to the incomplete fragments of type $D1_a$ and those of type $D0_{22}$.

The situation is quite different for Cu_3Au. The real structure just above T_c primarily contains two-dimensional microdomains of type LI_2 with a certain size distribution, approximately ranging between 1 and 6 unit cells. Although microdomains of type $D0_{22}$ or fragments thereof are also present, the proportion of these is less than in Ni_4Mo. The microdomains in all three alloys are embedded in a more-or-less-disordered matrix.

In order to compare the short-range-order parameters with the experimental results, a_{lmn} values were calculated from the 3D simulations and are presented in Table 5. Good agreement is obtained between the experimental and calculated a_{lmn} values except for a_{110} in the case of Ni_4Mo and Au_4Mn. This poor agreement is probably due to the difficulties of data correction, especially in the case for the nearest neighbours (a_{110}), as clearly pointed out by Hayakawa, Bardhan & Cohen (1975). In this context, it must be also noted that the a_{lmn} parameters calculated by the method of Gehlen & Cohen (1965) show, in any case, a better agreement because of the special type of simulation procedure which performs a fit between experimental and calculated a_{lmn} values. Both the experimental and calculated values of a_{200} and a_{211} exhibit a remarkable behaviour. In the case of Au_4Mn and Cu_3Au, the values of a_{200} are much larger than in the case of Ni_4Mo. In contrast to this, the values of a_{211} for Au_4Mn and Cu_3Au are smaller than those for Ni_4Mo. These facts are consistent with an increased generation of $D0_{22}$-type domains and fragments of $D1_a$-type domains during the short-range-order state of Ni_4Mo. The larger values of a_{200} in the case of Au_4Mn and Cu_3Au correspond to the generation of LI_2-type domains, which are rarely found in Ni_4Mo.

A structural interpretation using the a_{lmn} values is in this case possible because the described structures are visible in the videographic simulations, which are proven to be correct by the good agreement between their Fourier transforms and the experimentally measured diffuse diffraction intensities. A structural interpretation based only on the values of the short-range-order coefficients is not sufficient because each short-range-order coefficient represents a correlation length (Patterson function) which may correspond to different structure models.

The presented simulation procedure is also suitable for the structural characterization of defect distributions in crystal structures. A possible application is the correlation-vector-based description of the oxygen vacancy distribution in mullite, which obeys a certain ordering scheme (Rahman & Paulmann, 1991; Paulmann, Rahman & Weichert, 1992; Butler, Welberry & Withers, 1993; Rahman, 1994*b*). Moreover, it is also possible to convert the simulated videographic structure images into floating-point atomic coordinates (Rahman & Rodewald, 1991; Rodewald & Rahman, 1992) to enable image-contrast simulations to be carried out for interpreting the HREM images of a disordered structure.

References

Butler, B. D., Welberry, T. R. & Withers, R. L. (1993). *Phys. Chem. Mineral.* **20**, 323–332.

Chakravarti, B., Starke, E. A., Sparks, C. J. & Williams, R. O. (1974). *J. Phys. Chem. Solids*, **35**, 1317–1326.

Chen, H., Comostock, R. J. & Cohen, J. B. (1979). *Ann. Rev. Mater. Sci.* **9**, 51–86.

Cowley, J. M. (1950). *J. Appl. Phys.* **21**, 24–30.

Fuernrohr, P., Epperson, J. E. & Gerold, V. (1980). *Z. Metallkd.* **71**, 403–409.

Gehlen, P. C. & Cohen, J. B. (1965). *Phys. Rev.* **139**, 844–855.

Golosov, N. C. & Dudka, B. V. (1973). *Phys. Status Solidi B*, **59**, 361–366.

Gompper, G. & Kroll, D. M. (1988). *Phys. Rev. B*, **38**, 459–473.

Hayakawa, M., Bardhan, P. & Cohen, J. B. (1975). *J. Appl. Cryst.* **8**, 87–95.

Moss, S. C. (1964). *J. Appl. Phys.* **35**, 3547–3553.

Paulmann, C., Rahman, S. H. & Weichert, H.-T. (1992). European Congress on Electron Microscopy, Granada, Spain, Vol. 2, pp. 445–446.

Polgreen, T. L. (1985). *Acta Metall.* **33**, 185–189.

Rahman, S. H. (1993*a*). *Acta Cryst.* A**49**, 56–68.

Rahman, S. H. (1993*b*). *Acta Cryst.* A**49**, 68–79.

Rahman, S. H. (1994*a*). *Z. Kristallogr.* **209**, 315–321.

Rahman, S. H. (1994*b*). *Mullite and Mullite Ceramics*, edited by H. Schneider, K. Okada & J. A. Pask, pp. 4–31. London: Wiley.

Rahman, S. H. & Paulmann, C. (1991). *Optik (Stuttgart)*, Suppl. 4, **88**, 18.

Rahman, S. H. & Rodewald, M. (1991). *Optik (Stuttgart)*, Suppl. 4, **88**, 17.

Rodewald, M. (1993). Dissertation, Univ. Hannover, Germany.

Rodewald, M. & Rahman, S. H. (1992). Xth European Congress on Electron Microscopy, Granada, Spain, Vol. 1, pp. 537–538.

Saburi, T., Kanai, E. & Nenno, S. (1974). *J. Less-Common Met.* **37**, 59–70.

Suzuki, H., Harada, J., Nakashima, T. & Adachi, K. (1982). *Acta Cryst.* A**38**, 522–529.

Van Tendeloo, G. & Amelinckx, S. (1985). *Acta Cryst.* B**41**, 281–292.

Williams, R. O. (1970). Contract No. W-7405-eng-26, Metals and Ceramics Division, Oak Ridge National Laboratory, Tennessee, USA.

Zhu, X. M. & Zabel, H. (1990). *Acta Cryst.* A**46**, 86–94.